

RECEIVED: June 30, 2014 REVISED: August 25, 2014 ACCEPTED: September 26, 2014 PUBLISHED: November 20, 2014

12<sup>th</sup> Workshop on Resistive Plate Chambers and Related Detectors, 23–28 February 2014, Tsinghua University, Beijing, China

# Time of flight measurement in heavy-ion collisions with the HADES RPC TOF wall

# **HADES** collaboration

- G. Kornakov, $^{d,1}$  O. Arnold, $^{i,h}$  E.T. Atomssa, $^n$  C. Behnke, $^g$  A. Belyaev, $^f$
- J.C. Berger-Chen, i,h J Biernat, A. Blanco, C. Blume, M. Böhmer, P. Bordalo, a
- S. Chernenko, C. Deveaux, A. Dybczak, E. Epple, L. Fabbietti, D. Fateev,
- P. Fonte,<sup>a,2</sup> C. Franco,<sup>a</sup> J. Friese,<sup>i</sup> I. Fröhlich,<sup>g</sup> T. Galatyuk,<sup>d,3</sup> J.A. Garzón,<sup>p</sup> K. Gill,<sup>g</sup>
- M. Golubeva, D. González-Díaz, F. Guber, M. Gumberidze, d, S. Harabasz, d, b.
- T. Hennino,<sup>n</sup> C. Höhne,<sup>j</sup> R. Holzmann,<sup>c</sup> A. lerusalimov,<sup>f</sup> A. lvashkin,<sup>k</sup> M. Jurkovic,<sup>i</sup>
- B. Kämpfer, e,4 T. Karavicheva, K. Kardan, I. Koenig, W. Koenig, B. W. Kolb, c
- G. Korcyl, R. Kotte, A. Krása, E. Krebs, F. Krizek, H. Kuc, A. Kugler, T. Kunz,
- A. Kurepin,<sup>k</sup> A. Kurilkin,<sup>f</sup> P. Kurilkin,<sup>f</sup> V. Ladygin,<sup>f</sup> R. Lalik,<sup>i,h</sup> S. Lang,<sup>c</sup>
- K. Lapidus, i,h A. Lebedev, L. Lopes, M. Lorenz, L. Maier, A. Mangiarotti, A.
- J. Markert,<sup>g</sup> V. Metag,<sup>j</sup> J. Michel,<sup>g</sup> C. Müntz,<sup>g</sup> R. Münzer,<sup>i,h</sup> L. Naumann,<sup>e</sup> M. Palka,<sup>b</sup>
- V. Pechenov, O. Pechenova, V. Petousis, J. Pietraszko, W. Przygoda, b
- B. Ramstein,<sup>n</sup> L. Rehnisch,<sup>g</sup> A. Reshetin,<sup>k</sup> A. Rost,<sup>d</sup> A. Rustamov,<sup>g</sup> A. Sadovsky,<sup>k</sup>
- P. Salabura, T. Scheib, K. Schmidt-Sommerfeld, H. Schuldes, P. Sellheim, P. Salabura, P. Scheib, R. Schwidt-Sommerfeld, H. Schuldes, P. Sellheim, P. Salabura, P. Schwidt-Sommerfeld, H. Schuldes, P. Sellheim, P. Salabura, P. Schwidt-Sommerfeld, H. Schuldes, P. Sellheim, P. Salabura, P. Schwidt-Sommerfeld, H. Schuldes, P. Sellheim, P. Schwidt-Sommerfeld, P. Schwidt-S
- J. Siebenson, L. Silva, Yu.G. Sobolev, S. Spataro, H. Ströbele, J. Stroth, g.c
- P. Strzempek, C. Sturm, O. Svoboda, A. Tarantola, K. Teilab, P. Tlusty,
- M. Traxler, H. Tsertos, T. Vasiliev, V. Wagner, C. Wendisch, 4. J. Wirth, i.h.
- J. Wüstenfeld, S. Yurevich and Y. Zanevsky

<sup>&</sup>lt;sup>a</sup>LIP-Laboratório de Instrumentação e Física Experimental de Partículas, 3004-516 Coimbra, Portugal

<sup>&</sup>lt;sup>1</sup>Corresponding author.

<sup>&</sup>lt;sup>2</sup>Also at ISEC Coimbra, Coimbra, Portugal

<sup>&</sup>lt;sup>3</sup>Also at ExtreMe Matter Institute EMMI, 64291 Darmstadt, Germany

<sup>&</sup>lt;sup>4</sup>Also at Technische Universität Dresden, 01062 Dresden, Germany

```
<sup>b</sup>Smoluchowski Institute of Physics, Jagiellonian University of Cracow,
 30-059 Kraków, Poland
<sup>c</sup>GSI Helmholtzzentrum für Schwerionenforschung GmbH,
 64291 Darmstadt, Germany
<sup>d</sup>Technische Universität Darmstadt,
 64289 Darmstadt, Germany
<sup>e</sup>Institut für Strahlenphysik, Helmholtz-Zentrum Dresden-Rossendorf,
 01314 Dresden, Germany
<sup>f</sup> Joint Institute of Nuclear Research,
 141980 Dubna, Russia
<sup>g</sup>Institut für Kernphysik, Goethe-Universität,
 60438 Frankfurt, Germany
<sup>h</sup>Excellence Cluster 'Origin and Structure of the Universe',
 85748 Garching, Germany
<sup>i</sup>Physik Department E12, Technische Universität München,
 85748 Garching, Germany
<sup>j</sup>II.Physikalisches Institut, Justus Liebig Universität Giessen,
 35392 Giessen, Germany
<sup>k</sup>Institute for Nuclear Research, Russian Academy of Science,
 117312 Moscow, Russia
<sup>1</sup>Institute of Theoretical and Experimental Physics,
 117218 Moscow, Russia
<sup>m</sup>Department of Physics, University of Cyprus, 1678 Nicosia, Cyprus
<sup>n</sup>Institut de Physique Nucléaire (UMR 8608), CNRS/IN2P3 - Université Paris Sud,
 F-91406 Orsay Cedex, France
<sup>o</sup>Nuclear Physics Institute, Academy of Sciences of Czech Republic,
 25068 Rez, Czech Republic
<sup>p</sup>LabCAF. F. Física, Univ. de Santiago de Compostela,
 15706 Santiago de Compostela, Spain
<sup>q</sup>Dipartamento di Fisica Generale and INFN, Università di Torino,
 10125 Torino, Italy
```

E-mail: g.kornakov@gsi.de

ABSTRACT: This work presents the analysis of the performance of the RPC ToF wall of the HADES, located at GSI Helmholtzzentrum für Schwerionenforschung, Darmstadt. The behavior of the detector is studied in Au+Au collisions at 1.23 AGeV. A main characteristic of the detector is that all the active areas were designed to be electrically shielded in order to operate in high occupancies of the chambers. Here we show the achieved performance regarding efficiency and timing capabilities at different occupancies of this special design after the applied offline corrections to the data. Also the stability of the intrinsic time resolution over time of data taking is presented.

KEYWORDS: Resistive-plate chambers; Particle identification methods; Instrumentation and methods for time-of-flight (TOF) spectroscopy

#### **Contents**

1	Introduction  Performance of the detector in high multiplicity environment			1
2				2
	2.1	Time and position resolution of the detector		2
		2.1.1	Methods for offline calibration	3
		2.1.2	Time resolution dependence on occupancy of the detector	4
	2.2	Match	ing and intrinsic efficiency	4
		2.2.1	Intrinsic detector efficiency determined from matching efficiency	(
	2.3 Stability		7	
3	Conclusions			8

#### 1 Introduction

The HADES spectrometer [1], located at the SIS18 accelerator at GSI Helmholtzzentrum für Schwerionenforschung [2], Darmstadt, Germany, uses the technique of time of flight for particle identification. In the last years, the spectrometer was upgraded to be able to accomplish the goal of the experiment: the measurement of the rare and penetrating probes coming out of the collisions of heavy ions, such as gold, in the energy regime of few GeV per nucleon. This upgrade included the installation of a new time of flight wall made with Resistive Plate Chamber technology [3] in the inner part of the spectrometer, where the highest particle multiplicities, up to 200 charged particles per central collision, were expected. Therefore, the design and performance goals of the new detector were highly constrained by the geometry of an already existing subsystems and the required quality of particle identification. The relatively short path of particles from the target, and the densities expected in the most central collisions set a challenge to provide a detector with adequate granularity and very high time resolution.

After several tests [4, 5], the final layout was chosen. The detector was built in the following way: the total area of approximately 8 m<sup>2</sup> is divided in six sextants, called sectors. Each sector has trapezoidal shape and it is subdivided in three columns. Each column has 32 strip-like RPC cells read out on both sides, with 4 gaps of 280  $\mu$ m using glass as resistive material and aluminium electrodes as shown in the figure 1. In order to increase acceptance, efficiency and reduce dead regions, each column has two layers. The main characteristic of the detector, is that each independent RPC active area is electrically shielded in order to provide the smallest possible cluster size each time a charged particle crosses the detector. A more detailed description of the system and its operation parameters can be found in ref. [6].

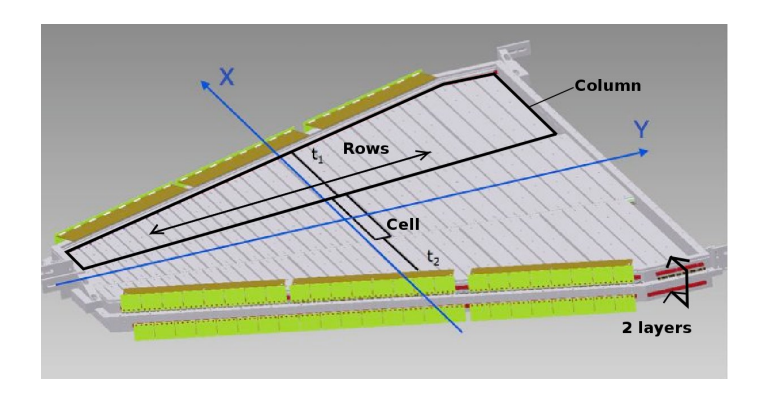
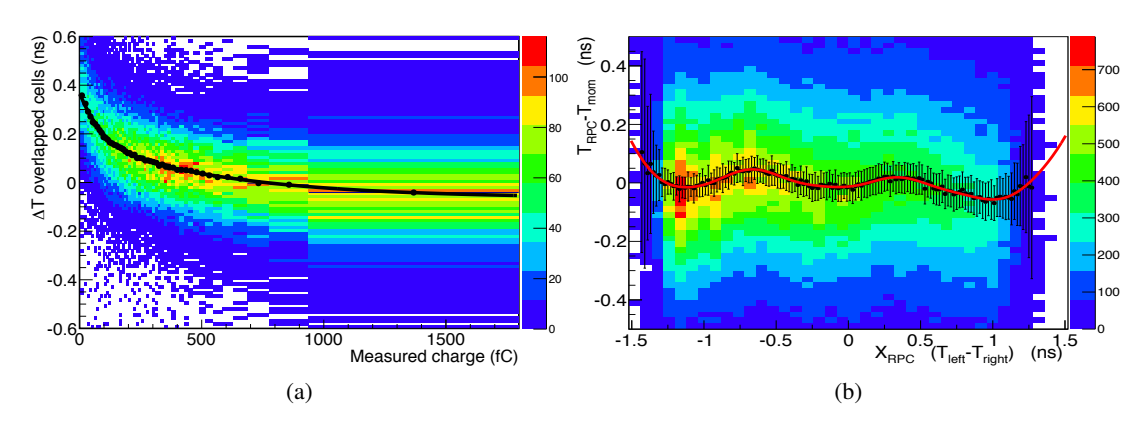


Figure 1. Internal structure of a HADES RPC sector and the reference coordinate system.



**Figure 2**. a) Time difference as a function of measured charge after pedestal subtraction. Example of the slewing correction or time-charge dependence fitted to two exponentials in order to compensate the systematic effect. b) Time difference between RPC ( $T_{rpc}$ ) and time reconstructed from tracking ( $T_{mom}$ ) as a function of a position in the RPC cell. Example of a position - time dependence of a RPC cell with the fit to a linear combination of five sinusoidal functions.

# 2 Performance of the detector in high multiplicity environment

The main goal of the detector is to operate in a high multiplicity environment and to provide excellent time resolution of the order of < 100 ps, and a longitudinal (x) position resolution as good as < 10 mm. Here we show the strategy for the offline data calibration and the detector performance from the point of view of stability, efficiency and resolution during the data production run of the HADES experiment occurred in April-May of 2012 (6 weeks in total), where Au+Au collisions at an energy of 1.23 GeV per nucleon were recorded.

# 2.1 Time and position resolution of the detector

The measured time  $(t_{meas})$  at each side can be decomposed in several terms: the time of flight of the particle  $(t_{ToF})$ , the time given by the diamond START detector  $(t_{start})$ , the time the signal is transported through the electrode to the FEE  $(t_s)$ , constant time sources that go to an offset term  $(t_o)$ 

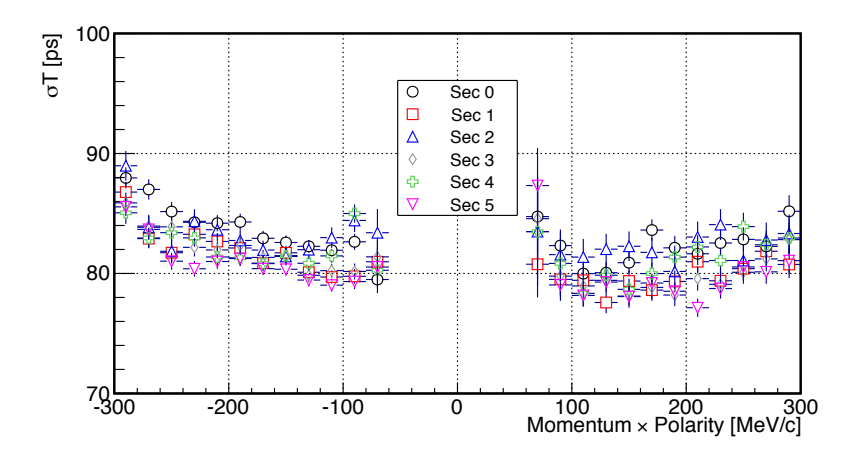


**Figure 3**. Time of flight resolution for electrons and positrons as a function of momentum measured by the HADES RPC ToF wall. Besides the intrinsic resolution of the RPC other sources such as the diamond START detector, length of the trace and multiple scattering are also present.

and finally a charge  $(\tau(q))$  and position  $(\tau(x))$  dependent parameters as shown in the equation (2.1):

$$t_{meas} = t_{ToF} + t_s + t_o - t_{start} + \tau(q) + \tau(x).$$
 (2.1)

The left-right measured times in the cell are merged into the half sum, or time of flight, and the half difference or position. Therefore, the corrections must be applied only to the combined values which represent the time of flight and the position, as some terms cancel after.

The internal structure of the detector allows to use the overlapped region between two cells belonging to the top and bottom layer to calculate intrinsic position and time resolution, i.e. the uncertainty coming from the detector itself and the electronic chain without other contributions to the measured time coming from uncertainties from the START detector or the particle path length.

Then, we define the intrinsic accuracy of one cell, under the assumption that both overlapping cells contribute in the same way to the uncertainty as:

$$\sigma_{X(up/down)} = \frac{1}{\sqrt{2}}\sigma(X_{RPC1} - X_{RPC2}). \tag{2.2}$$

Following the same strategy as the one used for position resolution, the intrinsic time resolution can be obtained by characterizing the distribution of time of flight differences between two overlapping cells. The results of the analysis of the intrinsic position resolution of all cells was already presented in ref. [7], showing 8 mm  $\sigma$  for the longitudinal position. The obtained mean time resolution is 64 ps  $\sigma$  and is studied below in section 2.3 from the point of view of the stability of the system.

#### 2.1.1 Methods for offline calibration

The charge-time correlation, or slewing correction, is compensated by two exponentials which describe the observed systematic deviation of the measured time. The exponential used to describe the region of low charges needs an extra parameter for the offset, requiring 5 parameters per cell

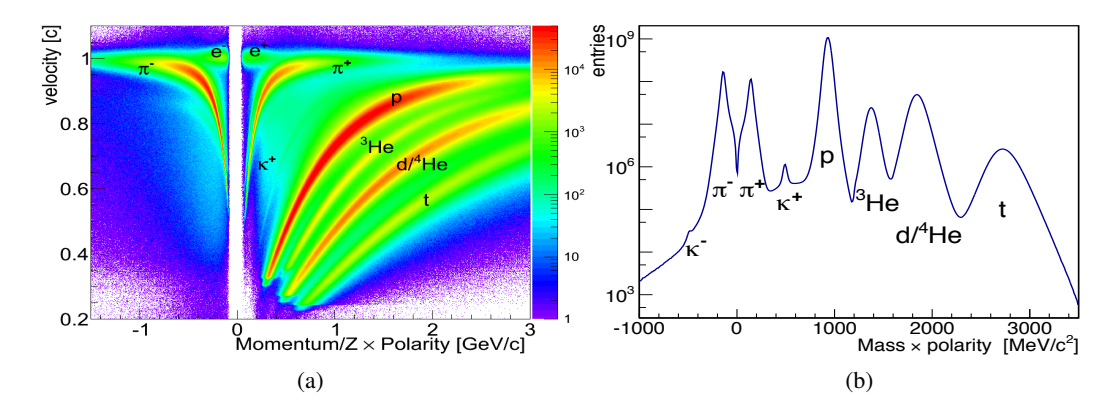


**Figure 4.** a) Velocity ( $\beta$ ) as a function of the particle momentum times polarity. The different particle species are shown with labels. b) Mass reconstructed from time of flight shows a very low background contamination.

as shown in the figure 2a. The correction is done using particles which have left signals in two overlapping cells from different layers by selecting events within a narrow charge window in one of the cells, used as reference for the other. Then, all the deviation in the distribution of time difference, can be assigned to the cell with unconstrained charge measurement. This procedure, is done recursively until convergence, which requires only two iterations.

The position dependent time offset is obtained using the measured hit position by the RPC. The  $\Delta T_{RPC-MDC}$  distribution is calculated by subtracting the calculated time of flight from tracking after particle's identification from the measured time by the RPC. Then, the dependence is corrected using a linear combination of five sinusoidal functions with different amplitudes and phase offsets, as shown in the figure 2b.

The synchronization of all the cells, that is the constant time offset determination, must provide the best separation capability between different particle species. The velocity versus momentum particle identification plots, obtained for each individual RPC cell, are merged all together into a single picture. However, the procedure to obtain these individual offsets is not trivial, as energy losses and scattering probability variate with emission angle, momentum and type of particle.

One of the main goals of the HADES experiment is to measure precisely dielectron spectra. The synchronization of the cells, therefore, was focused on charged pions in the momentum range where they start to overlap with electrons. Then, the individual time offsets were obtained by minimizing recursively the distribution  $\Delta T_{RPC-MDC}$  in the pion momentum range between 350 to 650 MeV/c until convergence.

The velocity resolution has other contributions besides the RPC intrinsic time of flight: uncertanties associated to the reaction time, measured by a diamond START detector and uncertainties coming from the particles path. Although electrons are more ionizing than MIPs they are the best probes for measuring track time resolution in HADES, as their velocity is not affected by scattering or energy loss processes and they travel through the spectrometer at the speed of light. The track time resolution is shown in figure 3 as a function of measured momentum. The mean time accuracy is 81 ps  $\sigma$  showing a very good performance of the whole time of flight system. The contribution

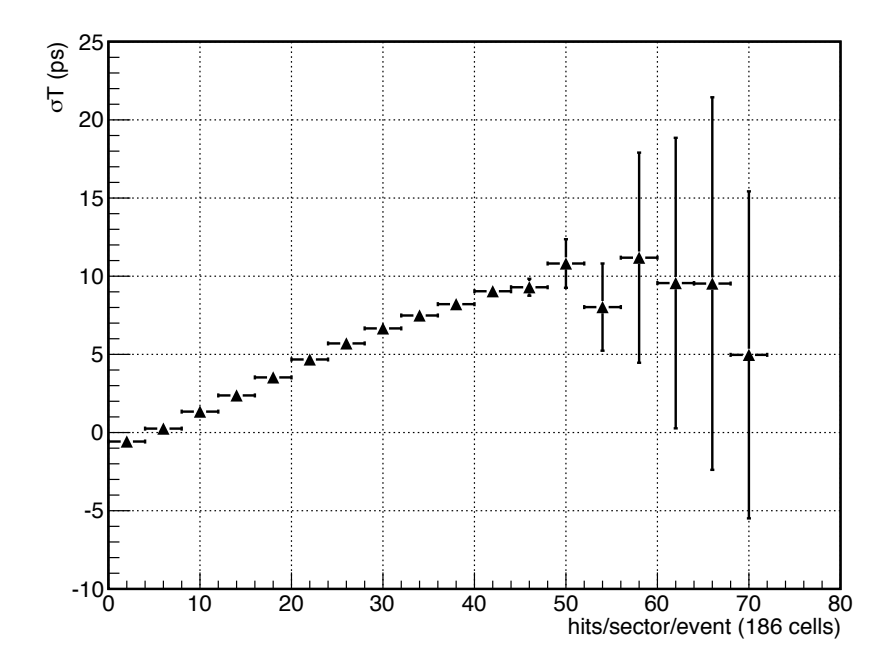


**Figure 5**. Effect of the multiplicity on the intrinsic time resolution on the HADES RPC. A worsening of 10 ps at occupancies larger than 30% was measured in heavy ion collisions, resulting in total for the highest multiplicities a time accuracy of 64 + 10 ps  $\sigma$ .

from the tracking detectors and the START is around 45 ps  $\sigma$ .

The resulting quality of the particle identification of the fully calibrated data is shown in the figures 4. The different particle species are clearly visible in a wide momentum range.

#### 2.1.2 Time resolution dependence on occupancy of the detector

Here we present the result of the analysis of the worsening of the time resolution as a function of particle multiplicity in each detector. This happens mostly due to the distortion of the charge measurement required for the slewing correction. In case that several particles generate avalanches in the same cell within the used integration time of the signal of 500 ns the collected charge is not any more correlated with the time measurement. This correction factor would be systematically shifted towards smaller values, see figure 2a, as the measured charge is larger that the real one.

The obtained worsening effect of the intrinsic time resolution for each multiplicity bin is shown in the figure 5. Contribution coming from an inhomogeneous velocity distribution for each multiplicity bin has been taken into account. There we can see a linear trend of 2 ps per 10 particles up to a multiplicity of 52 particles per sector, equivalent to an occupancy of 28%. For higher occupancies, large errors start to dominate and is not possible any more to precisely follow the trend, however it seems that it saturates close to the 10 ps value.

# 2.2 Matching and intrinsic efficiency

The matching efficiency determination of the detector can be obtained by performing a selection of traced particles by the tracking system to the Pre-Shower detector, located downstream and

covering the whole acceptance of RPC detector, without requiring an RPC signal in the track. Then, after obtaining the intersection point at the RPC plane, we loop through the recorded hits of the detector and identify if the cell was fired or not within a 50 mm window in the transversal and longitudinal directions, corresponding to a  $\sim 5\sigma$  window. Moreover, we have selected events with less than 10 particles in the studied sector in order to overcome systematic effects coming from occupancy. An almost flat distribution, where the disconnected cells are clearly visible, does not show any important issue or efficiency worsening (see for details ref. [7]).

## 2.2.1 Intrinsic detector efficiency determined from matching efficiency

After integrating all the six sectors into one single picture, as they are identical, the double layer structure starts to be visible. The areas covered by two overlapping cells appear with higher efficiency than those which are covered by one cell in one of the layers, as shown in the figure 6a.

From the amplitudes of the minima,  $\varepsilon_{\min}$ , and maxima,  $\varepsilon_{\max}$ , given by the matched efficiency calculation we can estimate the intrinsic efficiency of a cell using the following assumptions: there is an extrinsic factor  $\varepsilon_e$  and the efficiency  $\varepsilon_i$  of cells is assumed to be the same. Then we always can define the following system of equations:

$$\varepsilon_{\min} = \varepsilon_i \cdot \varepsilon_e$$
 (2.3)

$$\varepsilon_{\text{max}} = \left(1 - (1 - \varepsilon_i)^2\right) \cdot \varepsilon_e$$
 (2.4)

We can thus obtain the intrinsic efficiency of a single cell as follows:

$$\varepsilon_i = 2 - \frac{\varepsilon_{\text{max}}}{\varepsilon_{\text{min}}}. (2.5)$$

Figure 6a shows the matching efficiencies as a function of Y coordinate of the RPC sector. One can observe a two peak structure arising from the overlapping regions and places covered only by one cell instead of two. The minimum and maximum values as shown in the figure 6b are 0.94 and 0.99 respectively. Following equation (2.5) the single cell intrinsic efficiency is  $\varepsilon_i = 0.95$ . Taking into account that almost half is covered by two layers, the mean intrinsic efficiency of the detector is about 0.97.

As the RPC is one of the main subsystems for particle identification at small polar angles, the capability of an unbiased measurement of the efficiency as a function of particle type, momentum, incident angle is limited. The most pure sample can be obtained by selecting tracks with negative charge: there are mostly  $\pi^-$  and  $e^-$  present, and at momenta above 150 MeV/c the amount of negative pions strongly dominates (no anti-proton are produced at this energies). Considering additional power of discrimination provided by the specific energy loss measured by the MDC detectors, we can successfully reduce most of the contamination with a purity of 90% of pions in the sample. This is the only way of selecting particles without timing information from RPC detector.

This method is limited by the acceptance of negative particles, as the intense magnetic field bend them to the outermost region. Therefore study of the whole RPC surface is difficult. Nevertheless, it allows to perform a study of the dependency on the momentum of pions and their detection efficiency as a whole, independently of the RPC cell, which we can consider from the intrinsic study that provide a homogeneous response. Moreover, this method is useful to set the minimum

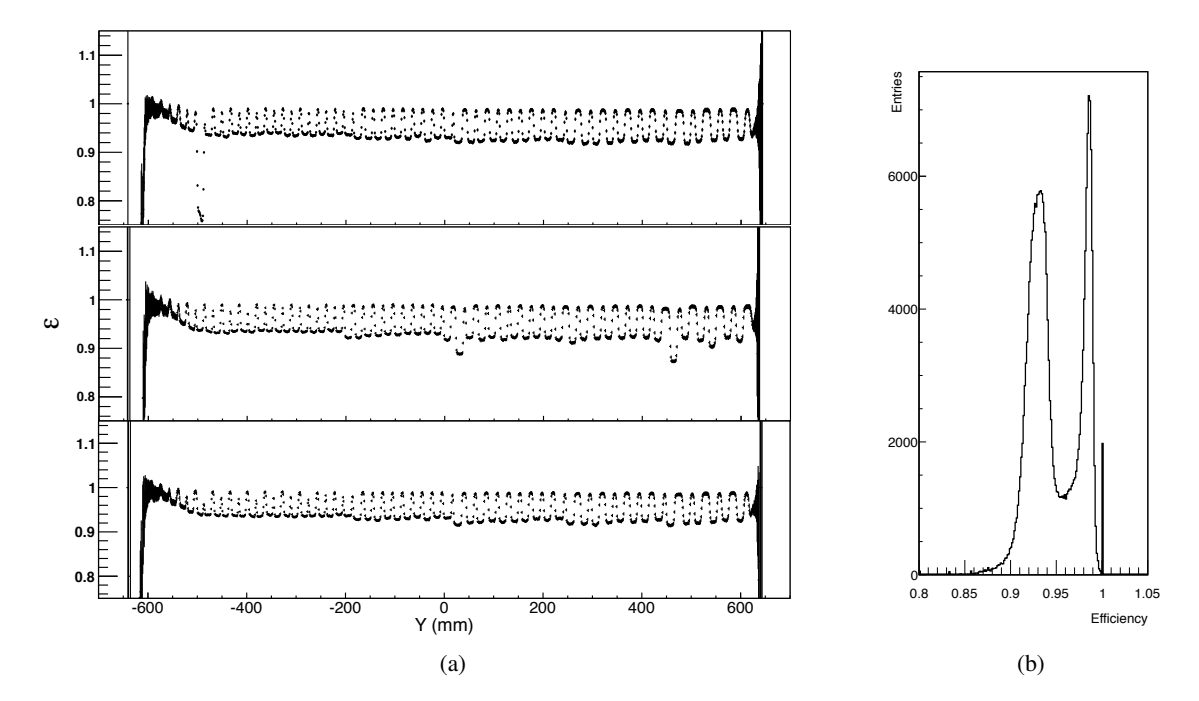


**Figure 6**. a) Projection along vertical axis Y of the matching efficiency for each of the three columns of one RPC sector, where the two layer structure creating the periodic structure is apparent. b) Efficiency values measured along the Y axis. This efficiency distribution allows to extract the location of the mean maximum (regions covered by two overlapping cells) and mean minimum (areas covered only by one cell) in order to calculate the intrinsic efficiency of the detector.

estimation of efficiency for MIPs particles, after taking into account some correction factor due to acceptance and extrinsic inefficiencies of the selected method, as shown in the figure 7. In that figure is clearly shown the relation between the primary ionization and the obtained efficiency, following a similar trend as the Bethe-Bloch curve does. The matching efficiency minimum,  $\varepsilon = 0.89$ , is located at the minimum ionizing region, i.e.  $\sim 450 \, \text{MeV/c}$  for pions.

## 2.3 Stability

The stability of the performance of the HADES RPC was studied over one month of intense radiation. The mean event rate was about 10 kHz, trigger was selecting 40% most central collisions. Seven billion Au+Au collisions were recorded. The accumulated charge after gas multiplication was about  $\sim$ 53 mC/cm². The chosen observable was the intrinsic timing accuracy, as it is the main observable of the quality of the data measured by the RPC used later in data analysis. This allowed to exclude deterioration coming from other possible sources unrelated to the detector itself, since only the information measured by the RPC is used. Figure 8 shows the obtained day-wise value for the whole data taking period during the 2012 campaign. The response is flat, around  $\sigma_T \approx 64 \pm 2$  ps, despite the first days where beam conditions were not fully stable and the chambers were being conditioned. Overall we can conclude that the performance of the chambers, in terms of time resolution was stable without anomalous observed behaviours.

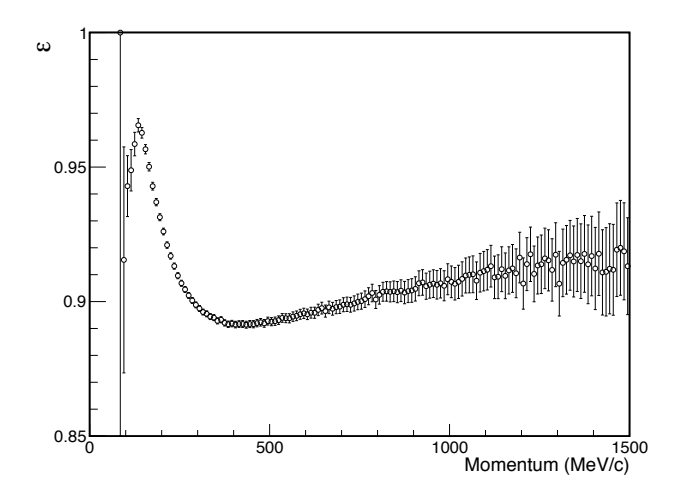


**Figure 7**. Matching efficiency as a function of momentum for negative pions. The shape of the curve shows a similar trend as the energy loss described by the Bethe-Bloch formula with minimum efficiency in the minimum ionizing region around 450 MeV/c for pions.

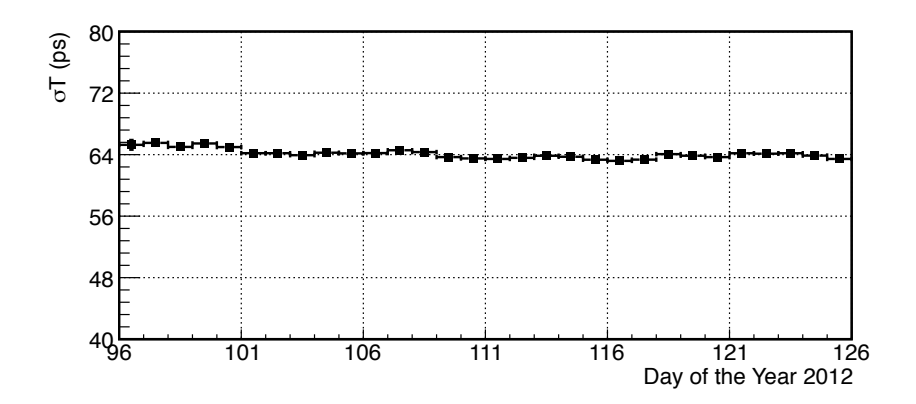


**Figure 8**. Time accuracy obtained over the period of data taking showing the stability of the detector response.

### 3 Conclusions

The operation of the HADES RPC ToF wall was stable during the beam time. Operation was done with constant settings, showing a stable performance over time. The measured times were calibrated and synchronised in order to provide the best identification capabilities for analysis. The performance study shows an overall efficiency of 97% and a mean intrinsic time accuracy of 64 ps  $\sigma$ . The mean electron track accuracy is 81 ps  $\sigma$  including contributions from START and tracking. Such performance allowed for the good particle identification in a wide momentum range.

## Acknowledgments

The HADES Collaboration gratefully acknowledges the support by PTDC/FIS/113339/2009 LIP Coimbra, NN202198639 SIP JUC Cracow, Helmholtz Alliance HA216/EMMI GSI Darmstadt, VH-NG-823, Helmholtz Alliance HA216/EMMI TU Darmstadt, 283286, 05P12CRGHE HZDR Dresden, Helmholtz Alliance HA216/EMMI, HIC for FAIR (LOEWE), GSI F&E Goethe-University, Frankfurt VH-NG-330, BMBF 06MT7180 TU München, Garching BMBF:05P12RGGHM JLU Giessen, Giessen UCY/3411-23100, University Cyprus CNRS/IN2P3, IPN Orsay, Orsay MSMT LG 12007, AS CR M100481202, GACR 13-06759S NPI AS CR, Rez, EU Contract No. HP3-283286.

#### References

- [1] HADES collaboration, G. Agakishiev et al., *The High-Acceptance Dielectron Spectrometer HADES*, *Eur. Phys. J.* A 41 (2009) 243 [arXiv:0902.3478].
- [2] GSI Helmholtzzentrum für Schwerionenforschung, https://www.gsi.de.
- [3] ALICE collaboration, P. Fonte, A. Smirnitsky and M.C.S. Williams, *A New high resolution TOF technology*, *Nucl. Instrum. Meth.* A **443** (2000) 201.
- [4] HADES collaboration, H. Alvarez-Pol et al., A large area timing RPC prototype for ion collisions in the HADES spectrometer, Nucl. Instrum. Meth. A 535 (2004) 277.
- [5] HADES collaboration, H. Alvarez-Pol et al., *Performance of shielded timing RPCs in a C-12 fragmentation experiment, Nucl. Instrum. Meth.* A 533 (2004) 79.
- [6] D. Belver et al., The HADES RPC inner TOF wall, Nucl. Instrum. Meth. A 602 (2009) 687.
- [7] A Blanco et al., *Performance of the HADES-TOF RPC wall in a Au + Au beam at 1.25 AGeV*, 2013 *JINST* **8** P01004.